Geosci. Instrum. Method. Data Syst. Discuss., doi:10.5194/gi-2016-39, 2016
Manuscript under review for journal Geosci. Instrum. Method. Data Syst.
Published: 8 December 2016

Geoscientific Instrumentation Methods and Data Systems
Discussions

Soil Salinity Mapping and Hydrological Drought Indices Assessment in Arid Environments Based on Remote Sensing Techniques

Mohamed Elhag and Jarbou A. Bahrawi

Department of Hydrology and Water Resources Management, Faculty of Meteorology,
Environment & Arid Land Agriculture, King Abdulaziz University
Jeddah, 21589. Saudi Arabia.

Correspondence to: melhag@kau.edu.sa

Abstract

Vegetation indices are mostly described as crop water derivatives. Normalized Difference Vegetation Index (NDVI) is one of the oldest remote sensing applications that widely used to evaluate crop vigor directly and crop water relationships indirectly. Recently, several NDVI derivatives are exclusively used to assess crop water relationships. Four hydrological drought indices are examined in the current research study. Water Supply Vegetation Index (WSVI), Soil Adjusted Vegetation Index (SAVI), Moisture Stress Index (MSI) and Normalized Difference Infrared Index (NDII) are implemented in the current study as an indirect tool to map the effect of different soil salinity level on crop water stress in arid environments. In arid environments; such as Saudi Arabia, water resources are under pressure especially groundwater levels. Groundwater wells are rapidly depleted due to the heavy abstraction of the reserved water. Heavy abstractions of groundwater; which exceed crop water requirements in most of the cases are powered by high evaporation rates in the designated study area because of the long days of extremely hot summer. Landsat OLI-8 data were extensively used in the current research to obtain several vegetation indices in response to soil salinity in Wadi Ad-Waser. Principal Component Analysis and Artificial Neural Network Analysis are complementary tools to understand the regression pattern of the hydrological drought indices in the designated study area.

Keywords: Arid Environment, Remote Sensing techniques, Soil Salinity Mapping, Vegetation Indices.

Geoscientific Instrumentation Methods and Data Systems Discussions
Open Access

1. Introduction

Remote sensing data considered to be a convenient source to perfume several vegetation indices in either simple or complicated band ratio combinations. Satellite images offer a large amount of data that could be analyzed, processed and stored to better understand several vegetation indices based on the type of the satellite sensor used (Govaerts et al., 1999; Pinty et al., 2009). Hypothetical backgrounds have been implemented to improve and enhance the optimization of particular satellite sensor to support certain vegetation indices (Verstraete et al., 1996; Gobron et al., 2000; Psilovikos and Elhag, 2013).

Spectral vegetation indices are mathematical combinations of different spectral bands mostly in the visible and near-infrared regions of the electromagnetic spectrum. Vegetation activities can be measured comprehensively through semi-analytical methods of spectral band ratios that have been extensively used to detect not only seasonal variability of the vegetation cover but also local scale spatial variability (Broge and Mortensen, 2002; Xiao et al., 2002).

The generic principle of utilizing vegetation indices is to improve the interpretation of the spectral data reflected from a vegetation cover. Spectral reflectance variabilities tend to differentiate between different vegetation characteristics based on crop water relationships and other surrounding features of soil components and atmosphere based on the maximization of vegetation characteristics over the surrounding environments (Moulin and Guerif, 1999; Boegh et al., 2002). Color, roughness, and water content are mainly the soil components that affect soil spectral reflectance (Curran, 1983a, b; Bouman and Tuong, 2001).

Soil parameter variation tends to draw a line on a plenary scattergram. Nevertheless, this line used as a reference point and known as “soil line” in vegetation studies involved both Red and Infrared spectral bands (Colombo et al., 2003, Elhag, 2014a, b). Utilization of vegetation indices

Geosci. Instrum. Method. Data Syst. Discuss., doi:10.5194/gi-2016-39, 2016
Manuscript under review for journal Geosci. Instrum. Method. Data Syst.
Published: 8 December 2016

Geoscientific Instrumentation Methods and Data Systems
Discussions
Open Access

has been challenged always by the major difficulty which is the minimization of soil component interferences and sensitivity maximization of atmospheric variations (Leprieur et al., 1994; Qi et al., 1994). Atmospherically Resistant Vegetation Index (ARVI) developed by Kaufman and Tanré (1992) and the Global Environmental Monitoring Index (GEMI) developed by Pinty and Verstraete (1991) are the less sensitive vegetation indices to the atmospheric variation. On the other hand, Qi et al. (1994) reported that the (GEMI) is soil noise sensitive. Higher noise sensitivity of GEMI has completely disabled the index and classifies it to arid region inadequate.

Implementations of vegetation indices are varied from a local leaf scale to continental vegetation scale. Moreover, certain indices tend to be site and/or species specific (Clevers, 1989; Elhag 2014a) and it can't be applied not only to different species but also different leave structure and canopies geometry (Xiao et al., 2002). Scholarly work of Kerr, and Ostrovsky (2003), Pettorelli et al. (2005), Huete et al. (2008) and Elhag (2014b) reported that several vegetation indices used to estimate different vegetation parameters extensively includes: Leaf Area Index (LAI), Fractional Vegetation Cover (FC), Crop Water Shortage Index (CWSI), Drought Severity Index (DSI) and Water Supply Vegetation Index (WSVI).

Soil salinization is a dynamic process arises basically when an excess of irrigational water is frequently used in the drainage capacity of the fields (Wardlow and Egbert, 2010). Implementations of remote sensing techniques in soil salinity mapping achieved comprehensive results on the regional scale (Montandon and Small, 2008). Brightness Index (BI), Normalized Difference Salinity Index (NDSI) and Salinity Index (SI), are widely distinguished in soil salinity mapping in an arid environment (Douaoui et al., 2006; Jiapaer et al., 2011). Current research aims to evaluate the suitability of different vegetation indices for a different level of remotely sensed soil salinity with contrasting to crop water relationships in Wadi Ad-Wasser.

2. Materials and methods

2.1. Study area

The study area, Wadi Ad Dawasir town is located in the plateau of Najd at Lat 44o 43' and Lon 20o 29'; about 300 km south of the capital city Riyadh. The study area illustrated in Figure 1 is comprised of gravelly tableland disconnected by insignificant sandy oases and isolated mountain bundles. Across the Arabian Peninsula as a whole, the tableland slopes toward the east from an elevation of 1,360 meters in the west to 750 meters at its easternmost limit. Wadi Ad Dawasir and Wadi ar Rummah the most important pattern of the ancient riverbeds remains in the study area. Wadi Ad Dawasir and Najran regions are the major irrigation water abstraction from Al-Wajid aquifer. Agriculture in Wadi Ad Dawasir area consists of technically highly developed farm enterprises that operate modern pivot irrigation system. The size of center pivot ranges from 30 ha to 60 ha with farms managing hundreds of them with the corresponding number of wells. The main crop grown in winter is wheat and occasionally potatoes, tomatoes or melons. All year fodder consists of alfalfa, which is cut up to 10 times a year for food. Typical summer crops for fodder are sorghum and Rhodes grass, which is perennial, but dormant in winter. The shallow alluvial aquifers could not sustain the high groundwater abstraction rates for a long time and groundwater level declined dramatically in most areas. Meteorological features of the area are speckled. Five elements of meteorology are constantly recorded through fixed weather station located within the study area. Temperature varies from 6^{o} C as minimum temperature to 43^{o} C as maximum temperature. Relative humidity is mostly stable at 24 %. Solar radiation of average sunrise duration is generally 11 hrs/day. Average wind speed is closer to 13 km/hr and may reach up to 46 km/hr in thunderstorm incidents. Finally, mean annual rainfall is about 37.6 mm (Al-Zahrani and Baig, 2011).

Figure 1. Location of the study area (Elhag, 2016).

2.2. Methodological framework

The current research work is based on assessing a regression correlation between different vegetation indices and their spatial corresponding soil salinity values conducted from satellite images. Principal Component Analysis is the undertaken tool to envisage the impacts of Soil Salinity on the current vegetation.

2.3. Estimation of vegetation indices

2.3.1. Water Supply Vegetation Index (WSVI):

$$WSVI = NDVI/T_s \quad (1)$$

Where

T_s is the brightness temperature channel or related remote sensing imagery estimated. The smaller this index is, the more severe the drought is.

2.3.2. Soil Adjusted Vegetation Index (SAVI):

$$SAVI = \frac{(NIR-R)}{(NIR+R)*(1+L)} \quad (2)$$

Where,

NIR is the Near Infrared band

R is the Red band

L is the is the soil brightness correction factor, commonly *L* = 0.5, (Huete, 1988).

Geoscientific Instrumentation Methods and Data Systems Discussions
Open Access

2.3.3. Moisture Stress Index (MSI):

$$MSI = \frac{SWIR_1}{NIR} \tag{3}$$

Where

SWIR₁ is the Short-wave Infrared band 1

NIR is the Near Infrared band

2.3.4. Normalized Difference infrared Index (NDII):

$$NDII = \frac{(NIR - SWIR_1)}{(NIR + SWIR_1)} \tag{4}$$

Where

NIR is the Near Infrared band

$SWIR_1$ is the Short-wave Infrared band 1.

2.4. Estimation of soil salinity index

Soil salinity indices are principally adjusted to detect salt mineral in soils based on the different responses of salty soils to various spectral bands. The following equation to map soil salinity was used after Elhag (2016):

$$SI = (G \times R)/B \tag{5}$$

Where,

B is the Blue band

G is the Green band

R is the Red band

Geoscientific Instrumentation Methods and Data Systems
Discussions

2.5. Regression Analyses

The purpose of the regression analyzes is to envisage the regression potentials between soil salinity index from one side and the rest of the hydrological drought indices from the other side. Principle Component Analysis (PCA) and Artificial Neural Network (ANN) were the implemented approaches. The PCA is to transform a set of likely correlated with unlikely correlated variables. Principal components number is less/equal to the variables original number. Following Lorenz (1956), PCA fundamental equations are:

First vector W $_{(1)}$ has to be answered as following:

$$w_{(1)} = \arg max_{\|w\|=1} \{\textstyle\sum_i (t_1)^2_{(i)}\} = \arg max_{\|w\|=1} \{\textstyle\sum_i (x_i \, . w)^2\} \tag{6}$$

The matrix form of the above equation gives the following:

$$w_{(1)} = \arg max_{\|w\|=1} \{\|Xw\|^2\} = \arg max_{\|w\|=1} \{w^T \, X^T \, Xw\} \tag{7}$$

W $_{(1)}$ has to be answered as following:

$$w_{(1)} = \arg max \left\{ \frac{w^T \, X^T \, Xw}{w^T \, w} \right\} \tag{8}$$

Originated $w_{(1)}$ suggests that first component of a data vector $x_{(i)}$ can then be expressed as a score of $t_{1(i)} = x_{(i)} \cdot w_{(1)}$ in the transformed co-ordinates, or as the corresponding vector in the original variables, $\{x_{(i)} \cdot w_{(1)}\} \, w_{(1)}$.

The neural network regression model is written as:

$$Y = \alpha + \textstyle\sum_h w_h \phi_h (\alpha_h + \sum_{i=1}^{p} w_{ih} X_i) \tag{9}$$

Where

$Y = E(Y|\boldsymbol{X})$. This neural network model has 1 hidden layer but it is possible to have additional hidden layers.

The $\phi(z)$ function used is hyperbolic tangent activation function. It's used for logistic activation for the hidden layers.

$$\phi(z) = \tanh(z) = \frac{1-e^{-2z}}{1+e^{-2z}} \tag{10}$$

It is significant that the final outputs to be linear not to constrain the predictions to be between 0 and 1. A simple diagram of a skip-layer neural network is illustrated in Figure 2. The equation for the skip-layer neural network for regression is shown below.

$$Y = \alpha + \sum_{i=1}^{p} \beta_i X_i + \sum_h w_h \phi_h(\alpha_h + \sum_{i=1}^{p} w_{ih} X_i) \tag{11}$$

It should be clear that these models are highly parameterized and thus, will tend to overfit the training data. Cross-validation is, therefore, critical to make sure that the predictive performance of the neural network model is adequate.

Figure 2. Artificial Neural Network scheme with 1 hidden layer and 3 nodes.

Recall the skip-layer neural network regression model looks like this:

$$Y = \alpha + \sum_{i=1}^{p} \beta_i X_i + \sum_h w_h \phi_h(\alpha_h + \sum_{i=1}^{p} w_{ih} X_i) \tag{12}$$

However, this model most likely overfits the training data. Consequently, determination of the adequate performance of the ANNs model is a must. Five different criteria are used: the Pearson coefficient of correlation (R), the root mean square error (RMSE), the mean absolute Deviation (MAD), the negative log-likelihood and the unconditional sum of squares (SSE). Basically, RMSE is the examined parameter for comparability reasons. RMSE can be computed as:

$$RMSE = \sqrt{\frac{1}{T_0} \sum_{t=1}^{T_0} (y_1 - \acute{y}_1)^2} \tag{13}$$

Where t is the time index, $\hat{y}_t$ and y_t are the simulated and measured values. Principally, the higher value of R and smaller values of RMSE ensure the better performance of the model.

3. Results and Discussion

Realization of the hydrological drought indices was exercised after a comprehensive remote sensing data correction. Basically, atmospheric correction and spatial enhancement were practiced utilizing Landsat 8 data acquired over the designated study area. The four hydrological drought indices were shown in Figures 3 to 6. Stochastic algorithms of WSVI and SAVI mapping (Figures 3 and 4) showed spatial coherence with a higher drought indices value within the agricultural area rather than the surrounding (Ceccato et al., 2001; Daughtry et al., 2004). On the contrary, MSI exercised as a deterministic drought index, it's nearly unaffected by changing water content. Conducted results showed two classes of stresses, stressed and no stress. The no stress class located within the agricultural area and the stressed area represented along the agricultural peripheral areas (Figure 5) where higher values indicate greater water stress and less water content. This could be explained rationally by the presence of irrigational sprinkles (Hunt et al., 1989; Ceccato et al., 2001). NDII is also a stochastic algorithm and was exercised in the current research due to the higher sensitivity of Infrared band to detect changes in water content of plant canopies (Hardisky et al., 1983). Spatial distribution of NDII (Figure 6) was mapped accordingly with WSVI and SAVI indices, in which higher NDII values means higher water content (Jackson et al., 2004). There are several algorithms to map soil salinity based on utilization of different remote sensing data as well as different ecological systems. An adequate NDSI algorithm was carried out according to Elhag (2016) findings in arid ecosystems. In Figure 7, NDSI was mapped in the designated study area showed spatial variation of salted soils, especially the new agricultural expansion at the southern west part of the designated study area due to the sprinkle movement drove the accumulation of excess waters at the peripherals of the agricultural areas (Lunetta et al., 2002; Konukcu et al., 2006).

Figure 3. Water Supply Vegetation Index (WSVI) thematic map over the study area.

Figure 4. Soil Adjusted Vegetation Index (SAVI) thematic map over the study area.

Figure 5. Moisture Stress Index (MSI) thematic map over the study area.

Figure 6. Normalized Difference Infrared Index (NDII) thematic map over the study area.

Figure 7. Normalized Difference Salinity Index (NDSI) thematic map over the study area.

Further statistical analyzes were carried out to construe the correspondences between salted soils and different horological drought indices. Regression analysis demonstrated in Figure 8 showed that salinity increases with lower WSVI and SAVI (Figure 8 a, b) which explained due to salt accumulation in soils. Under salinity stress conditions, there is no enough available water in soils for proper vegetation growth (Lunetta et al., 2002; Yang et al., 2011).

Generally, MSI values (Figure 8 c) are high in the study area because of the excess irrigation regime adopted to overcome the high evaporation rates (Elhag and Bahrawi, 2014; Elhag, 2016). Excess irrigation regimes in poor drain soils lead to waterlogging problems and salts accusation (Elhag, 2016).

Due to NDII higher sensitivity to water, NDII values increases with higher NDSI values. Salts accumulation caused by excessive irrigation is the driving force behind the proportional increment of NDII values in conjunction with NDSI values demonstrated in Figure 8d (Jackson et al., 2004; Shishi et al., 2015).

Geosci. Instrum. Method. Data Syst. Discuss., doi:10.5194/gi-2016-39, 2016
Manuscript under review for journal Geosci. Instrum. Method. Data Syst.
Published: 8 December 2016

Figure 8. Regression analyzes pf NDSI (ppm) against horological drought indices.

Figure 9 demonstrated the Principal Component Analysis along with the Factor Analysis. Moreover, eigenvalue decomposition is also demonstrated. WSVI and SAVI were grouped together. On the other hand, NDII and MSI were individually plotted against the former indices.

Figure 9. Principle Component Analysis.

Similar results conducted from the Scatter Plot Matrix and the companion correlation matrix shown in Figure 10 and Table 1. A high correlation is distinguished between WSVI and SAVI while negative correlation noted between WSVI and SAVI from one side and MSI AND NDII from the other side.

Figure 10. Scatterplot Correlation Matrix.

Table 1. Correlation matrix.

In Table 2, NDSI regression analysis shows that NDII is the proper fit based on different regression parameters (Rodgers and Nicewander, 1988). Spearman's correlation demonstrated in Table 3 supports PCA results. Hydrological drought indices were classified into two categories, MSI, and NDII in one category and WSVI and SAVI in the other one. The elements of each category are positively correlated. MSI and NDII were significantly correlated; WSVI and SAVI were highly correlated. Moreover, any other combinations of the four hydrological drought indices were not correlated.

The ANN analysis was carried out under 1 hidden layer, 3 nodes, and hyperbolic tangent activation function conditions. These conditions were carefully exercised to prevent the algorithm overfitting, ANN analysis is demonstrated in Table 4. NDII expressed the highest RMSE which indicates that NDSI and NDII are statistically the best fit ((Jiang, 2013). SAVI comes at the second best fit followed by WSVI. MSI failed to fit NDSI values comprehensively like the former hydrological drought indices (Jones and Marshall, 1992; Jiapaer et al., 2011).

Table 2. Regression analysis.

Table 3. Spearman's correlation.

Table 4. Neural Network Analysis .

4. Conclusion

The findings of the current research emphasized on the importance of the horological drought indices to envisage the adverse effects of salts accumulation in poorly drained soils. Remote Sensing techniques were satisfactory implement and interpreted in term of soil salinity mapping in consort with hydrological drought indices. Normalized Difference Infrared Index was statistically proved to be the Normalized Difference Salinity Index profound, followed by Soil Adjusted Vegetation Index and Water Shortage Vegetation Index respectively. Principal Component Analysis and Artificial Neural Network Analysis are complementary tools to understand the regression pattern of the hydrological drought indices in the designated study area. Further work needs to be considered towards the restrictiveness of the drastic effect of salts accumulation within the study area.

Acknowledgment

This work was supported by the Deanship of Scientific Research (DSR), King Abdulaziz University, Jeddah, under grant No. (155-36-1437D). The authors, therefore, gratefully acknowledge the DSR technical and financial support.

References

Al-Zahrani, K. H. and Baig, M. B. (2011). Water in the Kingdom of Saudi Arabia: Sustainable Management Options. The Journal of Animal and Plant Sciences, 21: 601– 604.

Bannari, A., Guedona, A. M., El-Hartib, A., Cherkaouic, F. Z. and El-Ghmari, A. (2008). Characterization of Slightly and Moderately Saline and Sodic Soils in Irrigated Agricultural Land using Simulated Data of Advanced Land Imaging (EO-1) Sensor. Communications in Soil Science and Plant Analysis, 39(19-20): 2795-2811.

Boegh, E., Soegaard, H., Broge, N., Hasager, C. B., Jensen, N. O., Schelde, K., and Thomsen, A. (2002). Airborne multispectral data for quantifying leaf area index, nitrogen concentration, and photosynthetic efficiency in agriculture. Remote Sensing of Environment, 81: 179–193.

Bouman B. A. M. and Tuong, T. P. (2001). Field water management to save water and increase its productivity in irrigated rice. Agricultural Water Management, 49(1):11-30.

Box, G. E. P. (1954). Some Theorems on Quadratic Forms Applied in the Study of Analysis of Variance Problems, II: Effects of Inequality of Variance and Correlation Between Errors in the Two-Way Classification. Annals of Mathematical Statistics, 1: 69-82.

Broge, N. H., and Mortensen, J. V. (2002). Deriving green crop area index and canopy chlorophyll density of winter wheat from spectral reflectance data. Remote Sensing of Environment, 81: 45–57.

Ceccato, P., Flasse, S., Tarantola, S., Jacquemoud, S. and Gregoire, J. M. (2001). Detecting vegetation leaf water content using reflectance in the optical domain. Remote Sensing of Environment, 77: 22–33.

Clevers, J. G. P. W. (1989). The application of a weighted infrared-red vegetation index for estimating leaf-area index by correcting for soil-moisture. Remote Sensing of Environment, 29: 25–37.

Colombo, R., Bellingeri, D., Fasolini, D. and Marino, C. M. (2003). Retrieval of leaf area index in different vegetation types using high resolution satellite data. Remote Sensing of Environment, 86: 120–131.

Curran, P. J. (1983a). Estimating green LAI from multispectral aerial-photography. Photogrammetric Engineering and Remote Sensing, 49: 1709–1720.

Curran, P. J. (1983b). Multispectral remote-sensing for the estimation of green leaf area index. Philosophical Transactions of the Royal Society of London Series a Mathematical Physical and Engineering Sciences, 309: 257–270.

Daughtry, C. S. T., Hunt Jr., E. R. and McMurtrey III, J. E. (2004). Assessing crop residue cover using shortwave infrared reflectance. Remote Sensing of Environment 90, 126–134.

Douaoui, A. K., Herve´, N. and Walter, C. (2006). Detecting salinity hazards within a semiarid context by means of combining soil and remote sensing data. Geodema, 134: 217–230.

Elhag, M. (2016). Evaluation of Different Soil Salinity Mapping Using Remote Sensing Techniques in Arid Ecosystems, Saudi Arabia. Journal of Sensors, 2016: 96175-96175.

Elhag, M. (2014a). Remotely Sensed Vegetation Indices and Spatial Decision Support System for Better Water consumption Regime in the Nile Delta. A Case Study for Rice Cultivation Suitability Map. Life Science Journal, 11(1): 201-209.

Elhag, M. (2014b). Sensitivity Analysis Assessment of Remotely Based Vegetation Indices to Improve Water Resources Management. Environment Development and Sustainability, 16(6): 1209-1222.

Elhag, M. and Bahrawi, J. (2014). Conservational Use of Remote Sensing Techniques for a Novel Rainwater Harvesting in Arid Environment. Environmental Earth Sciences, 72(12): 4995-5005.

Gobron, N., Pinty, B., Verstraete, M. M. and Widlowski, J. L. (2000). Advanced vegetation indices optimized for up-coming sensors: Design, performance, and applications. IEEE Transactions on Geoscience and Remote Sensing, 38: 2489–2505.

Govaerts, Y. M., Verstraete, M. M., Pinty, B. and Gobron, N. (1999). Designing optimal spectral indices: A feasibility and proof of concept study. International Journal of Remote Sensing, 20: 1853–1873.

Geosci. Instrum. Method. Data Syst. Discuss., doi:10.5194/gi-2016-39, 2016
Manuscript under review for journal Geosci. Instrum. Method. Data Syst.
Published: 8 December 2016

Hardisky, M., Klemas, V. and Smart, R. (1983). The influence of soil salinity, growth form, and leaf moisture on the spectral radiance of *Spartina alterniflora* canopies. Photogrammetric Engineering & Remote Sensing, 49: 77–83.

Huete, A., Didan, K., van Leeuwen, W., Miura, T. and Glenn, E. (2008). MODIS vegetation indices. In Land Remote Sensing and Global Environmental Change: NASA's Earth Observing System and the Science of ASTER and MODIS, 125 – 146.

Hunt, Jr. E.R., and Rock, B.N. (1989). Detection of changes in leaf water content using near- and middle infrared reflectances. Remote Sensing of Environment, 30: 43–54.

Jackson, T. J., Chen, D. Y., Cosh, M., Li, F. Q., Anderson, M., Walthall, C., Doriaswamya, P. and Hunt, Jr. R. E. (2004). Vegetation water content mapping using Landsat data derived normalized difference water index for corn and soybeans. Remote Sensing of Environment, 92, 475−482.

Jiang, B. (2013). Head/Tail Breaks: A New Classification Scheme for Data with a Heavy-Tailed Distribution. The Professional Geographer, 65(3): 482-494.

Jiapaer, G., Chen, X. and Bao, A. M. (2011). A comparison of methods for estimating fractional vegetation cover in arid regions. Agricultural and Forest Meteorology, 151(12): 1698–1710.

Jiapaer, G., Chen, X. and Bao, A. M. (2011). A comparison of methods for estimating fractional vegetation cover in arid regions. Agricultural and Forest Meteorology, 151(12): 1698–1710.

Jones, R. and Marshall, G. (1992). Land salinization, waterlogging and the agricultural benefits of a surface drainage scheme in Benerembah irrigation district. Review of Marketing and Agricultural Economics, 60: 173–189.

Kaufman, Y.J. and Tanré, D. (1992). Atmospherically resistant vegetation index (ARVI) for EOS-MODIS. Transactions on Geoscience and Remote Sensing, 30: 261–270.

Kerr, J. and Ostrovsky, M. (2003). From space to species: ecological applications for remote sensing. Trends in Ecology and Evolution, 18: 299-305.

Konukcu, F., Gowing, J. W. and Rose, D. A. (2006). Dry drainage: a sustainable solution to waterlogging and salinity problems in irrigation areas? Agricultural Water Management 83: 1–12, Konukcu, F., Gowing, J.W. and Rose, D.A. (2006). Dry drainage: A sustainable solution to waterlogging and salinity problems in irrigation areas? Agricultural Water Management, 83: 1-12.

Leprieur, C., Kerr, Y. H., Mastorchio, S. and Meunier, J. C. (2000). Monitoring vegetation cover across semi-arid regions: Comparison of remote observations from various scales. International Journal of Remote Sensing, 21(2):281–300.

Lorenz, E. N. (1956). Empirical orthogonal functions and statistical weather prediction. MIT Department of Meteorology, Statistical Forecast Project Rep. 1, 49 pp. [Available from Dept. of Meteorology, MIT, Massachusetts Ave., Cambridge, MA 02139.

Montandon, L. M. and Small, E. E. (2008). The impact of soil reflectance on the quantification of the green vegetation fraction from NDVI. Remote Sensing Environment, 112: 1835 – 1845.

Moulin, S. and Guerif, M. (1999). Impacts of model parameter uncertainties on crop reflectance estimates: A regional case study on wheat. International Journal of Remote Sensing, 20: 213–218.

Pettorelli, N., Vik, J., Mysterud, A., Gaillard, J., Tucker, C. and Stenseth, N. (2005). Using the satellite-derived NDVI to assess ecological responses to environmental change. Trends in Ecology and Evolution, 20: 503-510.

Pinty, B. abd Verstraete, M. M. (1992). GEMI: A non-linear index to monitor global vegetation from satellites. Plant Ecology, 101: 15–20.

Pinty, B., Lavergne, T., Widlowski, J. L., Gobron, N. and Verstraete, M. M. (2009). On the need to observe vegetation canopies in the near-infrared to estimate visible light absorption. Remote Sensing of Environment, 113: 10–23.

Psilovikos, A. and Elhag, M. (2013). Forecasting of Remotely Sensed Daily Evapotranspiration Data over Nile Delta Region, Egypt, Water Resources Management, 27(12): 4115-4130.

Qi, J., Chehbouni, A., Huete, A. R.; Kerr, Y. H. and Sorooshian, S. (1994). A modified soil adjusted vegetation index. Remote Sensing of Environment, 48: 119–126.

Rodgers, J. L. and Nicewander, W.A. (1988). Thirteen ways to look at the correlation coefficient. The American Statistician, 42 (1): 59–66.

Verstraete, M. M., Pinty, B. and Myneni, R. B. (1996). Potential and limitations of information extraction on the terrestrial biosphere from satellite remote sensing. Remote Sensing of Environment, 58: 201–214.

Wardlow, B. D. and Egbert, S. L. (2010). A comparison of MODIS 250-m EVI and NDVI data for crop mapping in the U.S. Central Great Plains. International Journal of Remote Sensing, 31(3): 805-830.

Xiao, X., He, L., Salas, W., Li, C., Moore, B., Zhao, R., Frolking, S. and Boles, S. (2002). Quantitative relationships between field-measured leaf area index and vegetation index derived from vegetation images for paddy rice fields. International Journal of Remote Sensing, 23: 3595–3604.

Yang, J. Y., Zheng, W., Tian, Y., Wu, Y. and Zhou, D. W. (2011). Effects of various mixed salt-alkaline stresses on growth, photosynthesis, and photosynthetic pigment concentrations of *Medicago ruthenica* seedlings. Photosynthetica, 49: 275-284.

Geosci. Instrum. Method. Data Syst. Discuss., doi:10.5194/gi-2016-39, 2016
Manuscript under review for journal Geosci. Instrum. Method. Data Syst.
Published: 8 December 2016

List of figures

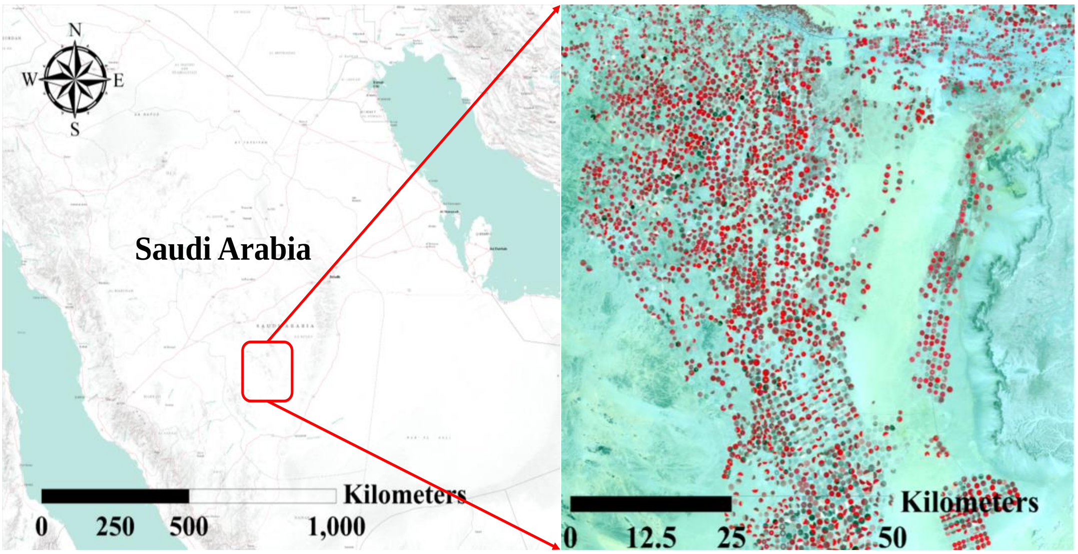

Figure 1. Location of the study area (Elhag, 2016).

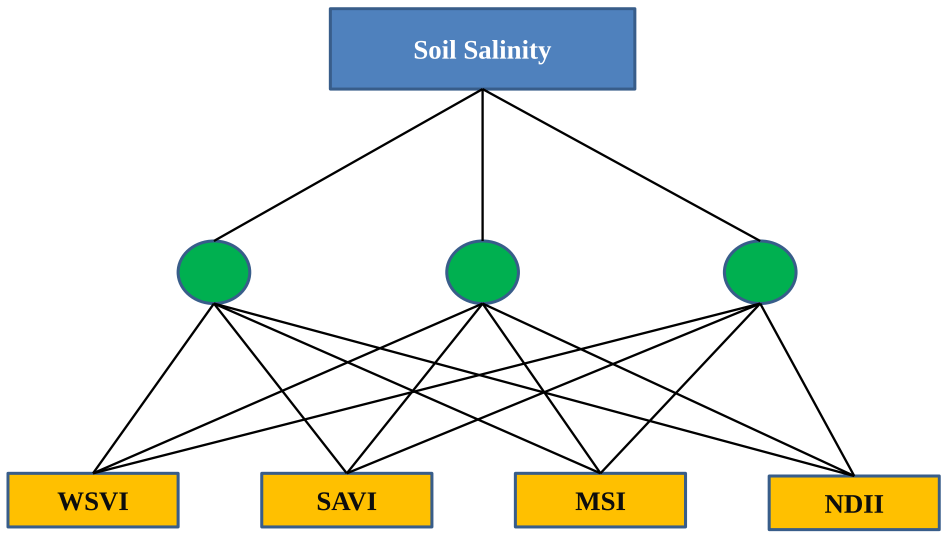

Figure 2. Artificial Neural Network scheme with 1 hidden layer and 3 nodes.

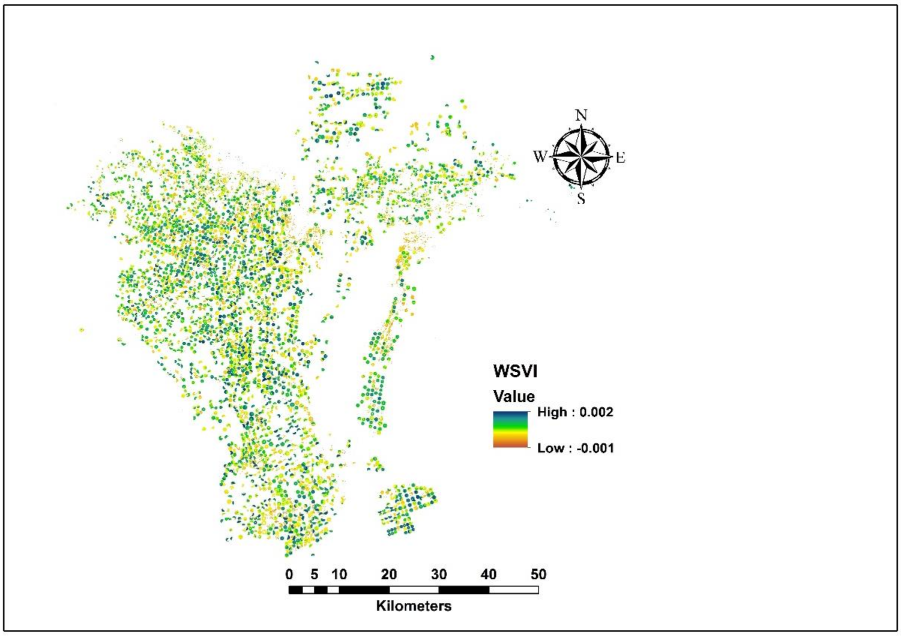

Figure 3. Water Supply Vegetation Index (WSVI) thematic map over the study area.

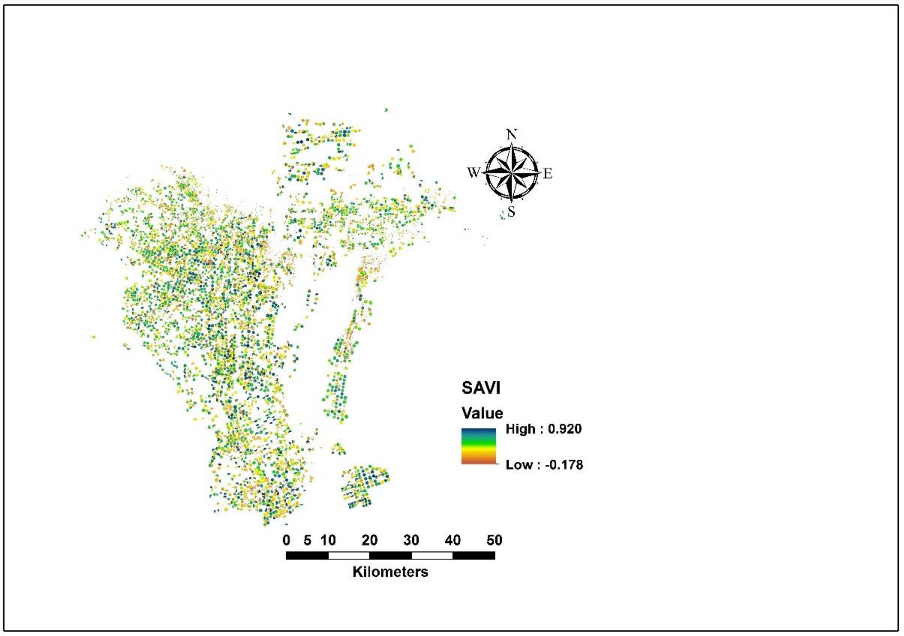

Figure 4. Soil Adjusted Vegetation Index (SAVI) thematic map over the study area.

Geosci. Instrum. Method. Data Syst. Discuss., doi:10.5194/gi-2016-39, 2016
Manuscript under review for journal Geosci. Instrum. Method. Data Syst.
Published: 8 December 2016

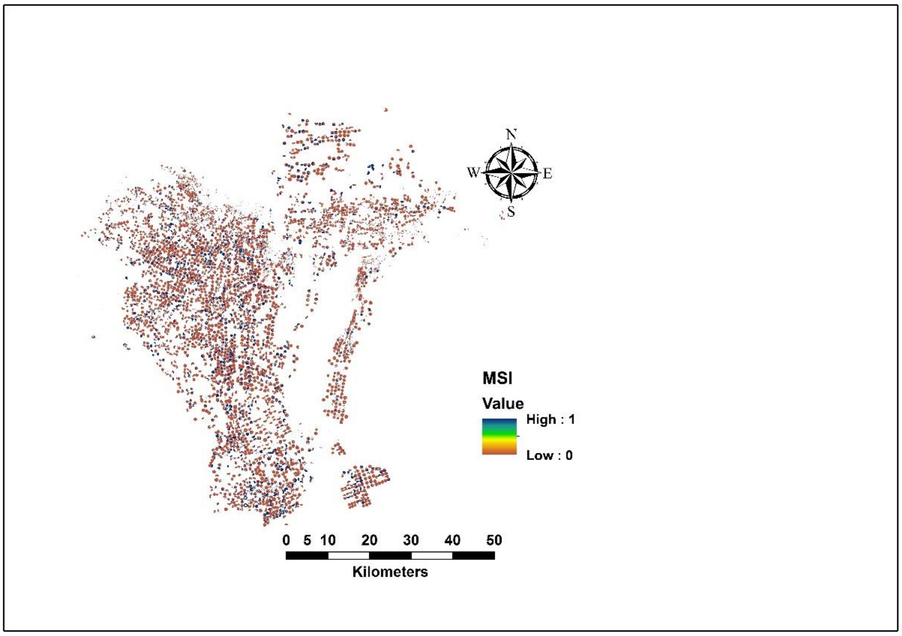

Figure 5. Moisture Stress Index (MSI) thematic map over the study area.

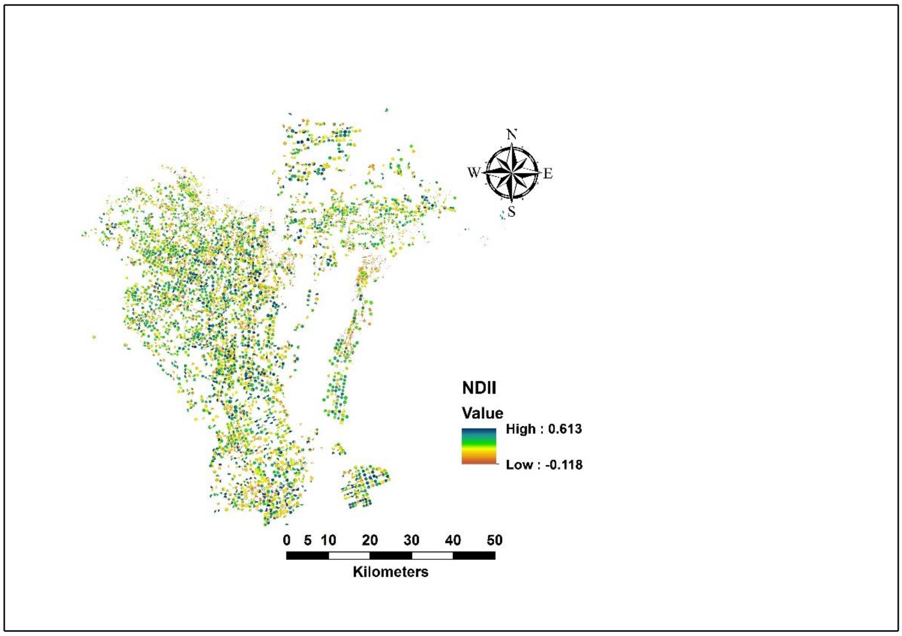

Figure 6. Normalized Difference Infrared Index (NDII) thematic map over the study area.

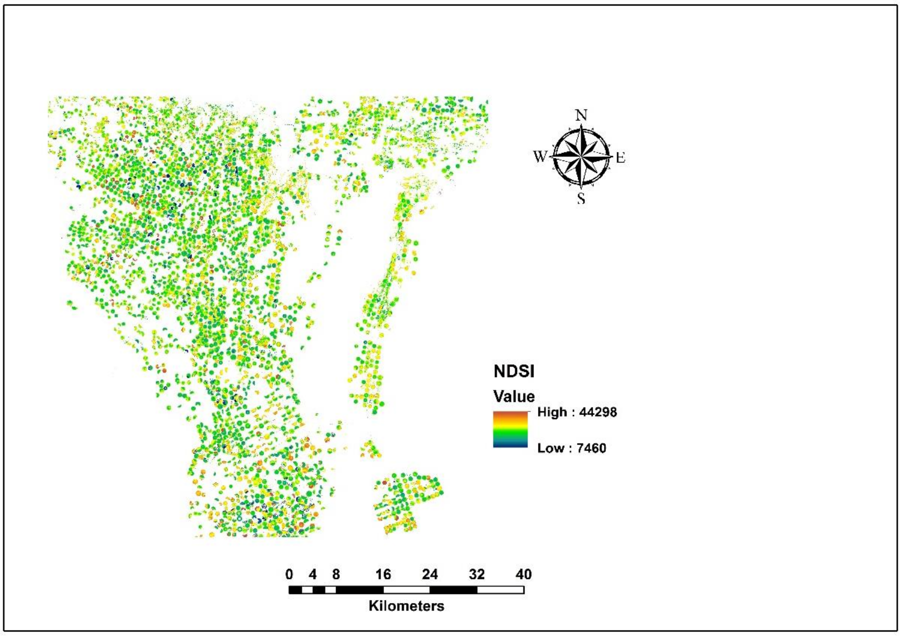

Figure 7. Normalized Difference Salinity Index (NDSI) thematic map over the study area.

461

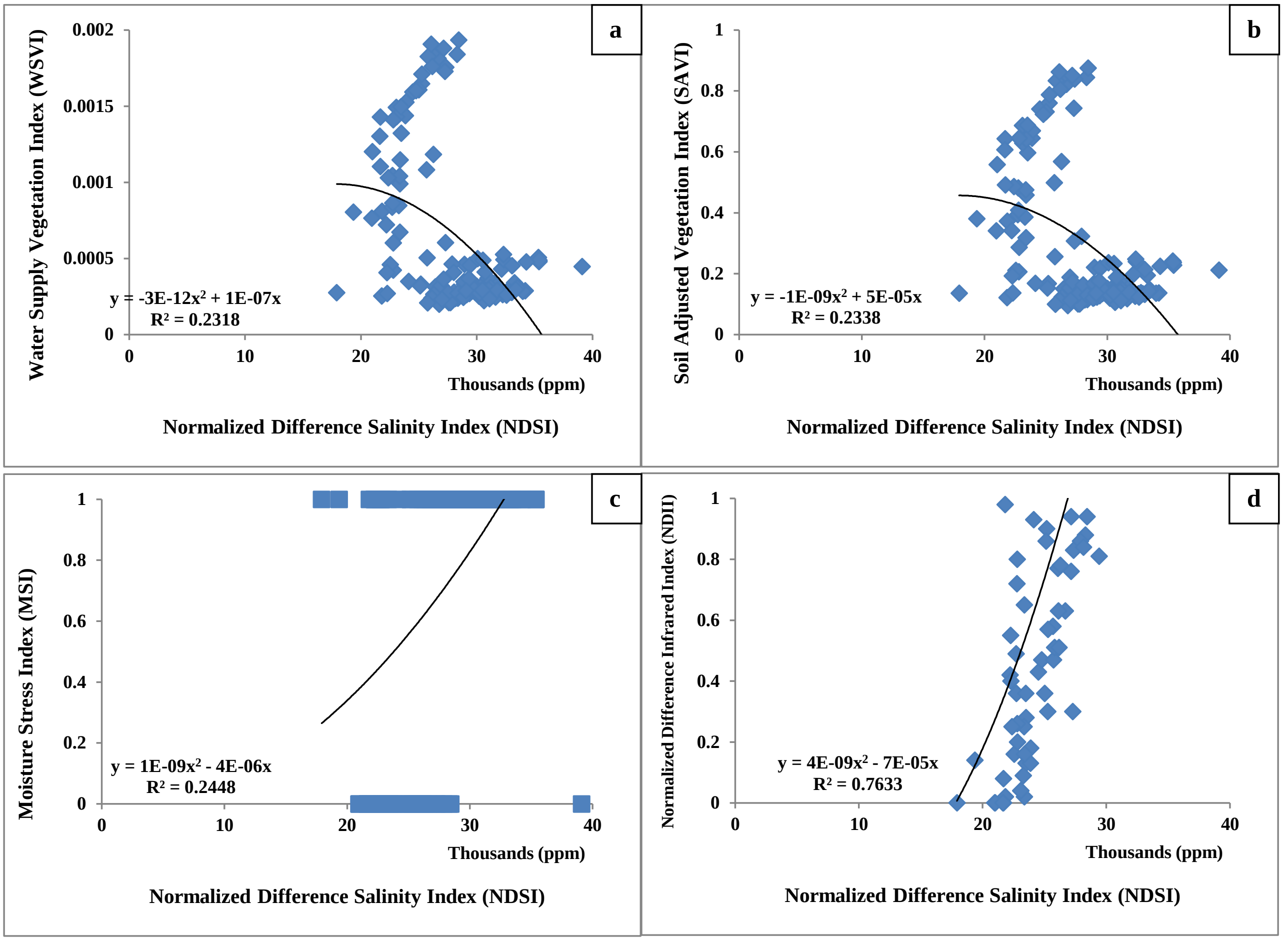

462

463 **Figure 8. Regression analyzes pf NDSI (ppm) against horological drought indices.**

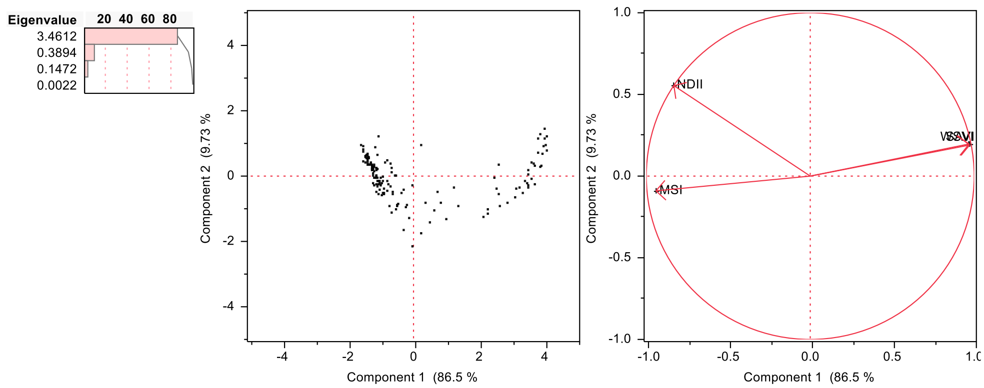

Figure 9. Principle Component Analysis.

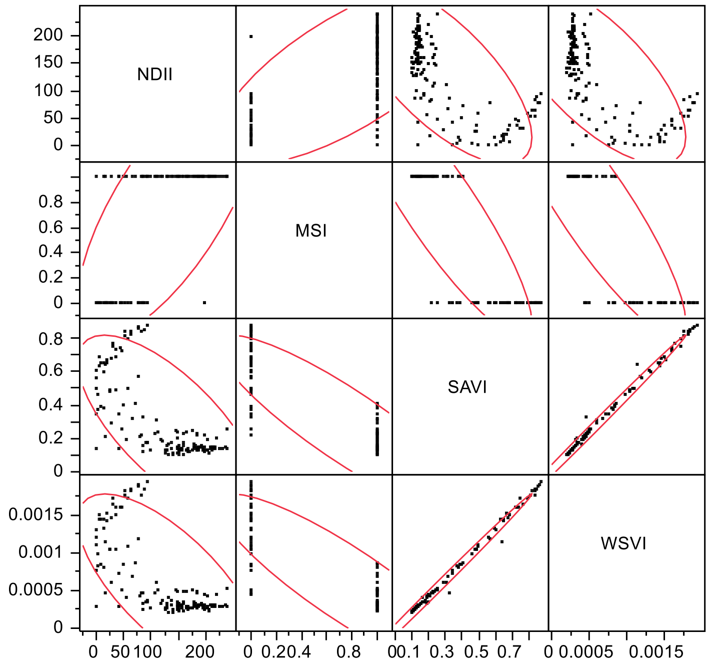

Figure 10. Scatterplot Correlation Matrix.

List of tables

Table 1. Correlation matrix.

	NDII	MSI	SAVI	WSVI
NDII	1	0.7182080406	-0.708975719	-0.703572559
MSI		1	-0.888156103	-0.88249756
SAVI			1	0.9977255509
WSVI				1

Table 2. Regression analysis.

	NDII	MSI	SAVI	WSVI
RSquare	0.798566127	0.254999657	0.246131379	0.243463225
RSquare Adj	0.797205088	0.249965871	0.241037672	0.23835149
Root Mean Square Error	31.88199207	0.384262574	0.202130562	0.000447112
Mean of Response	124.5466667	0.733333333	0.286361262	0.000611978
Observations (Sum Wgts)	150	150	150	150

Geoscientific Instrumentation Methods and Data Systems Discussions
Open Access

Table 3. Spearman's correlation.

Variable	By Variable	Correlation	Count	Lower 95%	Upper 95%	Significance probability
MSI	**NDII**	0.7182	150	0.6305	0.7878	*
SAVI	**NDII**	-0.7090	150	-0.7805	-0.6191	**NS**
SAVI	**MSI**	-0.8882	150	-0.9178	-0.8487	**NS**
WSVI	**NDII**	-0.7036	150	-0.7763	-0.6124	**NS**
WSVI	**MSI**	-0.8825	150	-0.9136	-0.8412	**NS**
WSVI	**SAVI**	0.9977	150	0.9969	0.9984	**

* is significant, ** is highly significant, NS is non-significant

Geosci. Instrum. Method. Data Syst. Discuss., doi:10.5194/gi-2016-39, 2016
Manuscript under review for journal Geosci. Instrum. Method. Data Syst.
Published: 8 December 2016

Geoscientific Instrumentation Methods and Data Systems Discussions
Open Access
EGU

Table 4. Neural Network Analysis.

		Training Measures	Validation Measures
NDII	RSquare	0.7574526	0.6698156
	RMSE	0.0999530	0.0972931
	Mean Abs Dev	0.0571881	0.0436599
	-LogLikelihood	-88.411680	-45.554430
	SSE	0.9990600	0.4732975
	Sum Freq	100	50
MSI	RSquare	0.3032101	0.0893892
	RMSE	0.2388872	0.1869959
	Mean Abs Dev	0.1203075	0.0628425
	-LogLikelihood	-1.2825260	-12.886510
	SSE	5.7067096	1.7483727
	Sum Freq	100	50
SAVI	RSquare	0.7565419	0.6698155
	RMSE	0.1499295	0.1459397
	Mean Abs Dev	0.0857822	0.0654899
	-LogLikelihood	-47.865170	-25.28115
	SSE	2.2478847	1.0649203
	Sum Freq	100	50
WSVI	RSquare	0.7533827	0.6619429
	RMSE	0.0003280	0.0003226
	Mean Abs Dev	0.0001876	0.0001451
	-LogLikelihood	-660.35100	-331.01460
	SSE	1.08E-05	5.20E-06
	Sum Freq	100	50